iScience

CellPress
OPEN ACCESS

Article

Robust ultrahigh electromagnetic interference shielding effectiveness based on engineered structures of carbon nanotube films

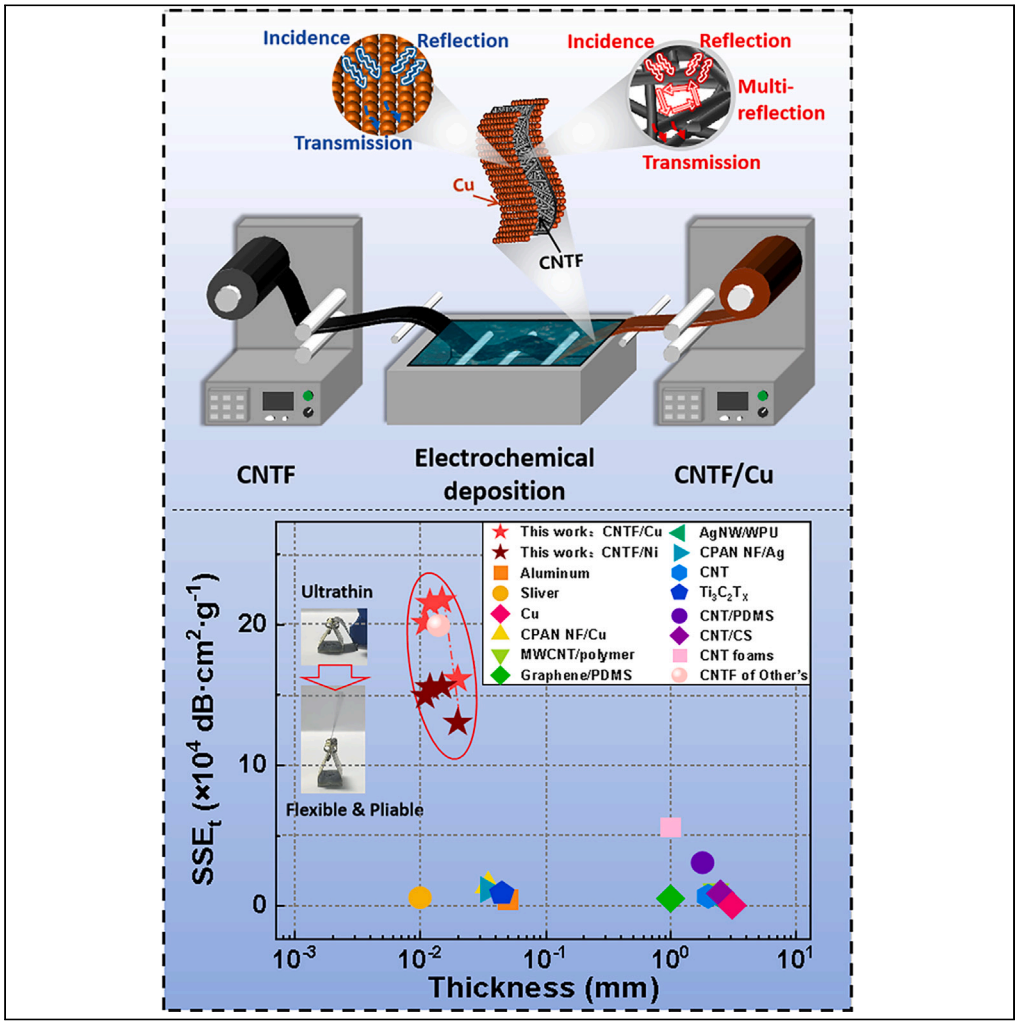

Haoxiang Zhang, Xiaojing Gong, Xucheng Dai, Zhenzhong Yong, Seeram Ramakrishna

gongxiaojing2018@cczu.edu.cn (X.G.)
zzyong2008@sinano.ac.cn (Z.Y.)
seeram@nus.edu.sg (S.R.)

Highlights

Composite materials are fabricated via a facile one-step electrodeposition method

Material property is enhanced by a combination of two shielding mechanisms

Composite films have excellent durability

Zhang et al., iScience 27, 109525
May 17, 2024
https://doi.org/10.1016/j.isci.2024.109525

iScience

CellPress
OPEN ACCESS

Article

Robust ultrahigh electromagnetic interference shielding effectiveness based on engineered structures of carbon nanotube films

Haoxiang Zhang,[1,4] Xiaojing Gong,[1,4,5,*] Xucheng Dai,[1] Zhenzhong Yong,[2,*] and Seeram Ramakrishna[3,*]

SUMMARY

High-performance electromagnetic interference (EMI) shielding materials with ultrathin, flexible, and pliable mechanical properties are highly desired for high-end equipments, yet there remain large challenges in the manufacture of these materials. Here, carbon nanotube film (CNTF)/copper (Cu) nanoparticle (NP) composite films are fabricated via a facile electrodeposition method to achieve high electromagnetic shielding efficiency. Notably, a CNTF/Cu NP composite film with 15 μm thickness can achieve excellent EMI shielding efficiency of ~248 dB and absolute EMI shielding effectiveness as high as 2.17×10^5 dB cm^2 g^{-1}, which are the best values for composite EMI shielding materials with similar or greater thicknesses. These engineered composite films exhibit excellent deformation tolerance, which ensures the robust reliability of EMI shielding efficiency after 20,000 cycles of repeated bending. Our results represent a critical breakthrough in the preparation of ultrathin, flexible, and pliable shielding films for applications in smart, portable and wearable electronic devices, and 5G communication.

INTRODUCTION

With the rapid development of 5G mobile communication and portable electronic devices, the electromagnetic interference (EMI) problem becomes an increasingly serious problem that both severely impacts the performance of electronic products and equipment and contributes to environment EMI pollution.[1–5] The drive to miniaturize smart and portable electronic devices requires flexible and ultrathin EMI materials.[6–10] To solve these problems, efforts have targeted the development of ultrathin high-performance EMI shielding materials that are effective against high-energy and wide-frequency radiation.[11–19]

As shown in Figure 1, traditionally, metal and carbon materials have been widely used as EMI shielding materials. Metals, such as copper (Cu) and nickel, are common for this purpose; however, their shallow skin depth results in high surface reflection. Therefore, they cannot be used as wave-absorbing materials. In addition, the metal sheets are bulky, costly, and prone to corrosion, so they are not suitable for use in lightweight electronic products.[20] High-magnetic-permeability alloys have also been considered as EMI shielding materials due to their high relative permeability and light weight, but their high stiffness, susceptibility to corrosion, and high cost limit their practical application.[21] Intrinsically conductive polymers have been studied as EMI shielding materials due to their low density and absorption-dominated shielding mechanism (which is more desirable in stealth technology); however, they have poor mechanical and thermal properties which limit their practical use.[22] In this regard, carbon nanotube films (CNTFs) and their composites are considered to be the best candidates for flexible and ultrathin EMI shielding materials, because they possess excellent conductivity and are lightweight, flexible, and chemically inert.[23–25] In 2021, the hierarchical macro-to-micro pore structure and properties of carbon nanotube (CNT) foam were tailored over a wide range via a secondary chemical vapor deposition (CVD) process. Benefiting from the multilevel reflection in hierarchical pore structures, optimized CNT foam achieves a high shielding efficiency (SE) of 84 dB and an absolute SE (SSE_t) of 5.6×10^4 dB cm^2 g^{-1}. The thicknesses of these pure CNT foams are typically in the range of the 1–10 mm.[26] An ultrathin densified CNTF was fabricated by purification via concentrated sulfuric acid and subsequent densification. The EMI SE of the CNTF reached 101 dB with a film thickness of 14.7 μm. The SSE_t was as high as 1.9×10^5 dB cm^2 g^{-1}. However, the densification process uses concentrated strong sulfuric acid, which limits its batch production.[27]

Here, we report on an engineered sandwich-structured CNTF/Cu nanoparticle (NP) composite film with excellent EMI shielding performance. All freestanding composite films are fabricated by an easy and facile electrochemical deposition method. Inspired by long-plate effect, EMI shielding effectiveness is enhanced by a combination of two shielding mechanisms. The excellent EMI shielding efficiency is attributed to the engineered sandwich structure of CNTF/Cu NP composite films, which have a high reflection efficiency on the outside of the Cu

[1]Institute of Materials Science and Engineering, Changzhou University, Changzhou 213164, P.R. China
[2]Division of Advanced Nanomaterials, Suzhou Institute of Nano-Tech and Nano-Bionics, Chinese Academy of Sciences, Suzhou 215123, China
[3]Center for Nanofibers and Nanotechnology, National University of Singapore, Singapore 117576, Singapore
[4]These authors contributed equally
[5]Lead contact
*Correspondence: gongxiaojing2018@cczu.edu.cn (X.G.), zzyong2008@sinano.ac.cn (Z.Y.), seeram@nus.edu.sg (S.R.)
https://doi.org/10.1016/j.isci.2024.109525

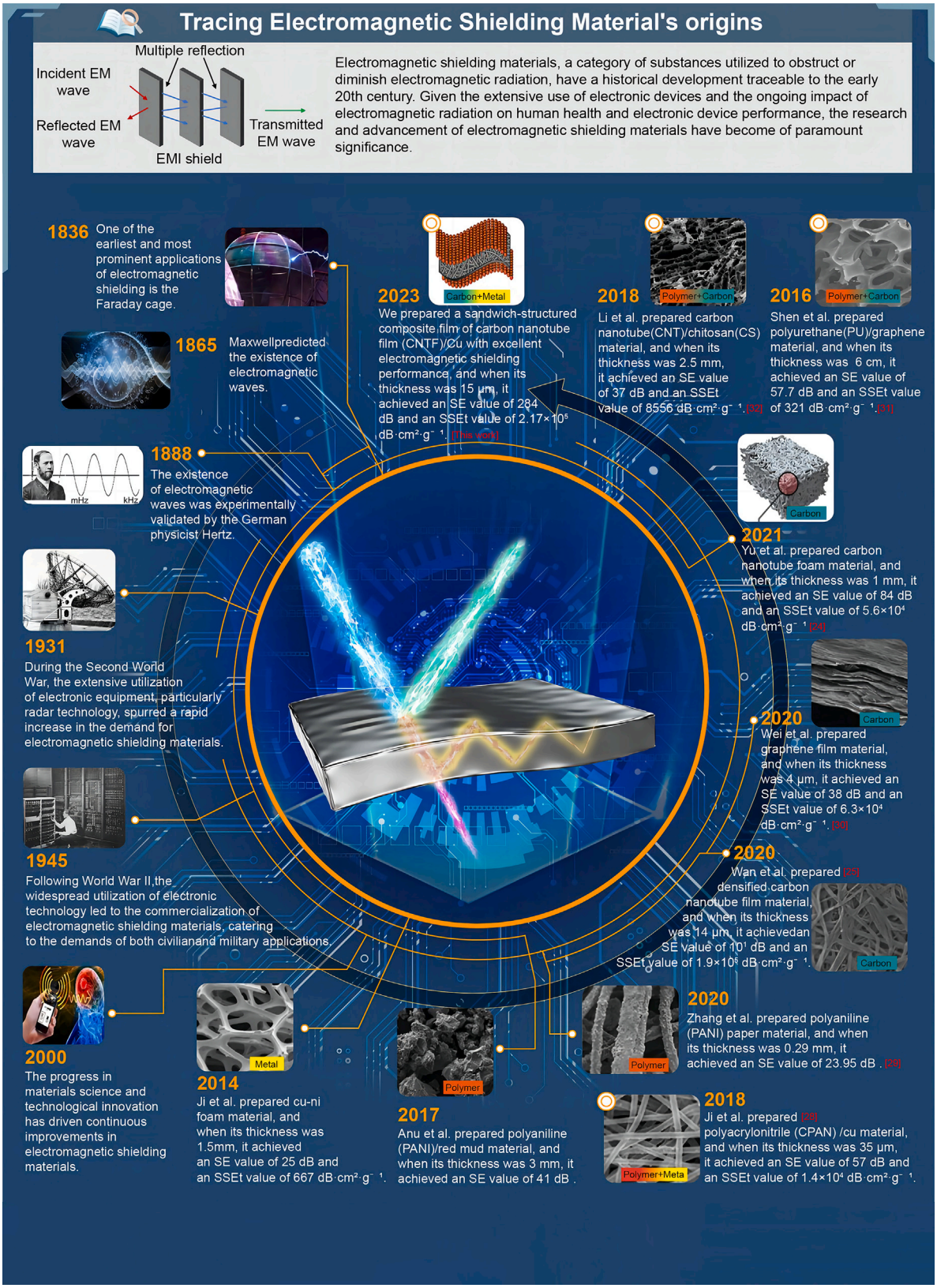
Tracing Electromagnetic Shielding Material's origins
Multiple reflection
Incident EM wave
Reflected EM wave
Transmitted EM wave
EMI shield
Electromagnetic shielding materials, a category of substances utilized to obstruct or diminish electromagnetic radiation, have a historical development traceable to the early 20th century. Given the extensive use of electronic devices and the ongoing impact of electromagnetic radiation on human health and electronic device performance, the research and advancement of electromagnetic shielding materials have become of paramount significance.
1836 One of the earliest and most prominent applications of electromagnetic shielding is the Faraday cage.
1865 Maxwellpredicted the existence of electromagnetic waves.
1888 The existence of electromagnetic waves was experimentally validated by the German physicist Hertz.
mHz
kHz
1931 During the Second World War, the extensive utilization of electronic equipment, particularly radar technology, spurred a rapid increase in the demand for electromagnetic shielding materials.
1945 Following World War II,the widespread utilization of electronic technology led to the commercialization of electromagnetic shielding materials, catering to the demands of both civilianand military applications.
2000 The progress in materials science and technological innovation has driven continuous improvements in electromagnetic shielding materials.
2014 Ji et al. prepared cu-ni foam material, and when its thickness was 1.5mm, it achieved an SE value of 25 dB and an SSEt value of 667 dB·cm²·g⁻¹.
Metal
2017 Anu et al. prepared polyaniline (PANI)/red mud material, and when its thickness was 3 mm, it achieved an SE value of 41 dB .
Polymer
2018 Ji et al. prepared [28] polyacrylonitrile (CPAN) /cu material, and when its thickness was 35 μm, it achieved an SE value of 57 dB and an SSEt value of 1.4×10⁴ dB·cm²·g⁻¹.
Polymer+Meta
2020 Zhang et al. prepared polyaniline (PANI) paper material, and when its thickness was 0.29 mm, it achieved an SE value of 23.95 dB . [29]
Polymer
2020 Wan et al. prepared [25] densified carbon nanotube film material, and when its thickness was 14 μm, it achievedan SE value of 10¹ dB and an SSEt value of 1.9×10⁵ dB·cm²·g⁻¹.
Carbon
2020 Wei et al. prepared graphene film material, and when its thickness was 4 μm, it achieved an SE value of 38 dB and an SSEt value of 6.3×10⁴ dB·cm²·g⁻¹. [30]
Carbon
2021 Yu et al. prepared carbon nanotube foam material, and when its thickness was 1 mm, it achieved an SE value of 84 dB and an SSEt value of 5.6×10⁴ dB·cm²·g⁻¹ [24]
Carbon
2016 Shen et al. prepared polyurethane(PU)/graphene material, and when its thickness was 6 cm, it achieved an SE value of 57.7 dB and an SSEt value of 321 dB·cm²·g⁻¹.[31]
Polymer+Carbon
2018 Li et al. prepared carbon nanotube(CNT)/chitosan(CS) material, and when its thickness was 2.5 mm, it achieved an SE value of 37 dB and an SSEt value of 8556 dB·cm²·g⁻¹.[32]
Polymer+Carbon
2023 We prepared a sandwich-structured composite film of carbon nanotube film (CNTF)/Cu with excellent electromagnetic shielding performance, and when its thickness was 15 μm, it achieved an SE value of 284 dB and an SSEt value of 2.17×10⁵ dB·cm²·g⁻¹. [This work]
Carbon+Metal

Figure 1. The introduction figure about the origin and development of EMI shielding materials

High-performance EMI shielding materials with ultrathin, flexible, and pliable mechanical properties are highly desired and very difficult to be fabricated. The future trending for high-efficiency EMI shielding materials is composite materials combining together the long-plate effect of different kinds of materials, such as polymer-metal composite materials, carbon fiber and metal composite materials, carbon nanomaterials and metal composite materials.[26–34]

NP layers and the multi-reflection and adsorption efficiency from CNTF in the middle layer. Specifically, the prepared sandwich CNTF (with densified thickness of 10 μm)/Cu composite film, with a deposition time of 60 min (~5 μm thickness), exhibits an ultrahigh EMI SE of approximately 248 dB at a structure thickness of approximately 15 μm. Our SSE_t is as high as 2.17×10^5 dB cm^2 g^{-1}. To the best of our knowledge, our reported EMI SE values are the best values achieved for composite EMI shielding materials with similar or greater thicknesses, and they are also higher than the reported EMI SE values of typical pure metals. In addition, these light-weight, ultra-thin CNTF/Cu NP composite films also have excellent, flexible and pliable mechanical properties, which ensure that they can maintain their the electromagnetic shielding effectiveness even after repeated bending over 20,000 cycles. This work provides a new approach for developing high-performance, ultrathin, flexible, and pliable EMI shielding materials that can be applied in various fields.

RESULTS AND DISCUSSION

Design principle and structural characterizations

Figure 2A shows ultra-thin and flexible CNTF/Cu NP composite films are fabricated via easy and facile one-step electrochemical deposition. A CNT sheet is drawn from a rotating CNTF roll, passed through a deposition bath, and finally collected on a winder. It should be noted that our continuous method can be stably scaled up. As we known, when electromagnetic waves pass through a shielding material, part of the wave is reflected at the surface of the material, and the remaining part enters the shield material, travels forward, and continues to weaken until it passes through the material. The shielding mechanism arises from the surface reflection loss on the interface of the material, the absorption loss of the material, and multiple reflection losses within the material. For pure metal, its shallow skin depth results in high surface reflection. Hence, when electromagnetic waves pass through metallic materials, they are mainly dissipated in the form of reflection loss (as shown in the enlarged images of Figure 2A).

For a CNTF or CNT foam, multiple reflections and absorption play the key role. The multiple reflections are due to the reflection and scattering of electromagnetic waves at various uneven interfaces within the EMI shielding material. When electromagnetic waves pass through CNTFs, due to their unique porous structure, they are reflected multiple times within the film and are mainly dissipated in the form of absorption loss (as shown in the enlarged images of Figure 2A). Traditional metal or carbon EMI shielding materials require a sufficient thickness to

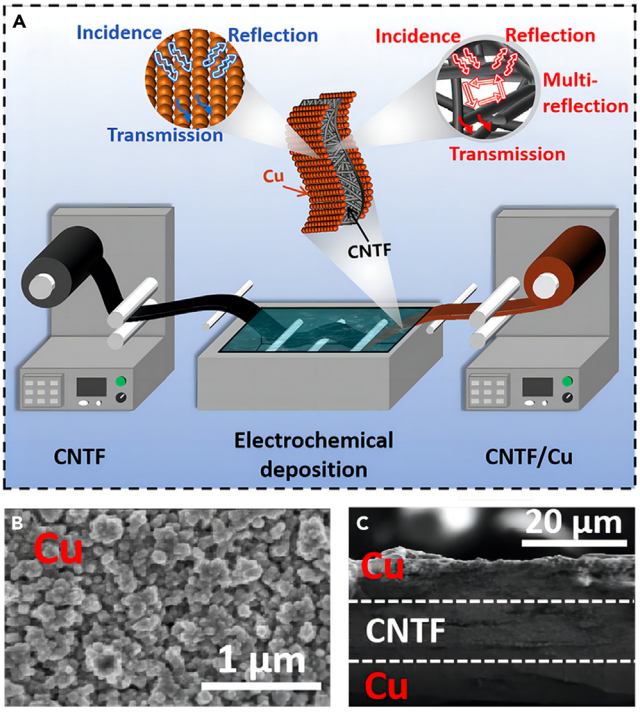

Figure 2. Conceptual design, and fabrication process of composite films

(A) Conceptual design and fabrication process of CNTF/Cu NP composite films.

(B and C) Top (B) and cross-section (C) SEM view of layered CNTF/Cu NP composite film.

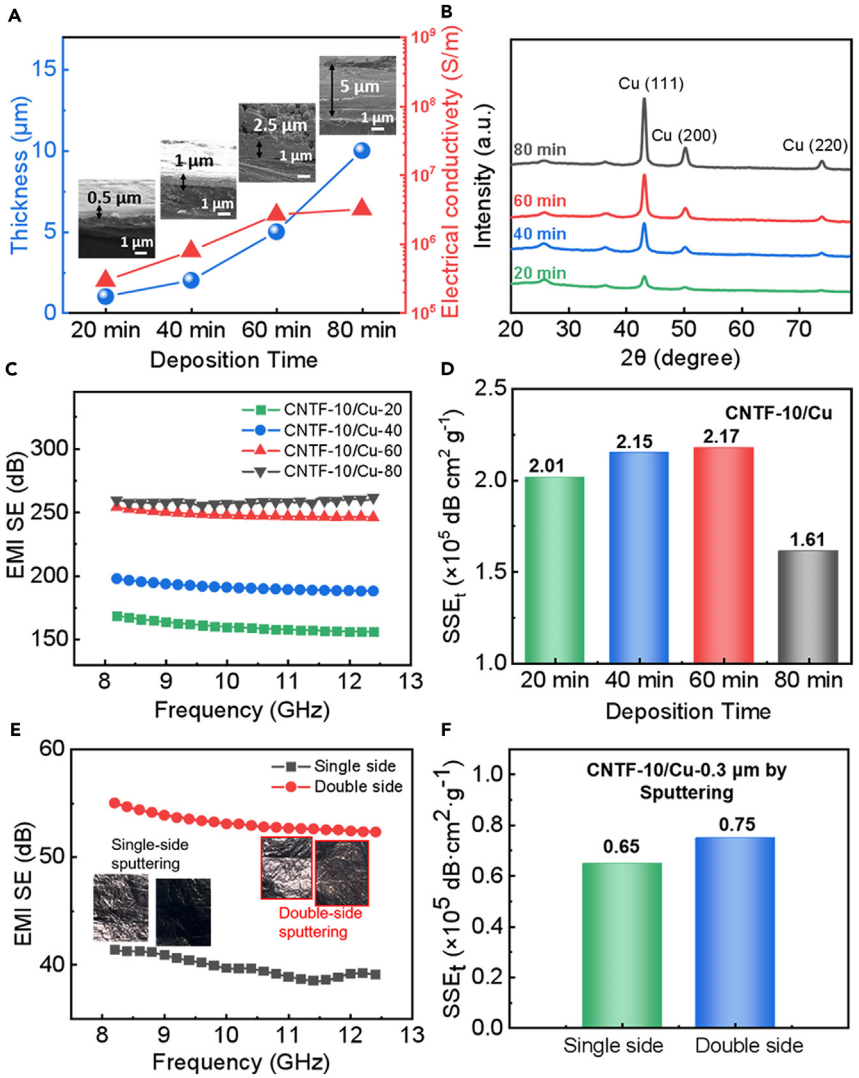

Figure 3. Electromagnetic shielding performance of composite thin films

(A) Metal layer thickness (blue line) and conductivity of composites (red line) under different electrochemical deposition times.

(B) X-ray analysis for CNTF-10/Cu with different electrodeposition times.

(C) Electromagnetic shielding performance testing of CNTF-10/Cu with different electrodeposition times.

(D) The normalized specific shielding efficiency SSE_t of CNTF-10/Cu with different electrodeposition times. SSE_t = SE/(density × thickness).

(E) Electromagnetic shielding performance of single and double sided copper sputtering.

(F) Absolute electromagnetic shielding performance of single and double sided copper sputtering.

dissipate more radiation. Hence, it is very difficult to achieve ultrathin materials with high values of SE and SSE_t by using traditional EMI shielding materials. In this work, by combining the advantages of the two dominating shielding mechanisms in metal and CNTF materials, we designed and engineered a sandwich-structured composite film of Cu NP/CNTF/Cu NP to achieve enhanced EMI shielding performance.

Characterization of conductibility, EMI shielding efficiency, and mechanical properties

As an inherent property of electromagnetic shielding materials, conductivity is a key factor affecting the electromagnetic shielding efficiency, because it affects the materials' reflection and absorption properties. Hence, we first explore the influence of the thickness of the Cu NP layer on the EMI efficiency. We electrochemically deposited Cu NP layers with different thicknesses on CNTF with densified thickness of 10 μm. The blue line in Figure 3A shows the thickness changes in the Cu NP layer corresponding to different chemical deposition times. With an increase in electrochemical deposition time, the conductivity increases linearly (as shown by the red line in Figure 3A). The conductivities of CNTF-10/Cu-20 and CNTF-10/Cu-40 were 1.92 × 10^5 S/m and 7.85 × 10^5 S/m, respectively. The reaction time was doubled, whereas the conductivity of the composite nanofiber membrane increased by a factor of four. For CNTF-10/Cu-60, the conductivity reached 2.65 × 10^6 S/m, which is one

Table 1. The comparison of SE and SSE_t for CNTF and CNTF/Cu systems

Material	CNTF-10	CNTF-10/Cu-20	CNTF-10/Cu-40	CNTF-10/Cu-60	CNTF-10/Cu-80
SE (dB)	38	160	191	248	258
SSE_t (dB cm^2 g^{-1})	76000	201740	215381	217830	161250

order higher than that of CNTF-10/Cu-40 and CNTF-10/Cu-20. When the reaction time was further extended to 80 min, the conductivity only slightly increased. The detailed top-view and side view of SEM images for CNTF/Cu at different electroplating times are shown in Figures S1 and S2. Higher conductivity increases the performance of electromagnetic shielding. X-ray diffraction (XRD) analysis confirmed the formation of Cu NPs. The XRD spectra of the CNTF/Cu NP composite films show that a typical Cu face-centered cubic structure is formed in the composite films. As the electrochemical deposition time increases, the peak intensity of the diffraction peaks gradually increases. The XRD peaks of CNTF/Cu at $2\theta = 43.29°$, 50.43°, and 74.13° correspond to the reflections of the (111), (200), and (220) crystal planes of the face-centered cubic structure of metal Cu (corresponding to the standard pattern of Cu, JCPDS (Joint Committee on Powder Diffraction Standards) card number: 04-0836),[35] as shown in Figure 3B.

We further tested the electromagnetic shielding efficiency of these composite films at the X-band. The electromagnetic shielding efficiencies corresponding to CNTF-10/Cu-20, CNTF-10/Cu-40, CNTF-10/Cu-60, and CNTF-10/Cu-80 are shown in Figure 3C. The EMI SE was clearly observed to increase as the electrochemical deposition time increased from 20 to 80 min (data shown in Table 1, detailed data shown in Figure S3), which is consistent with the trend of their electrical conductivities. However, when considering the density of the whole materials, the system with the highest absolute value of normalized specific SE (SSE_t) is the CNTF-10/Cu-60 system (in Figure 3D). This is mainly because, with the reaction time increasing, the thickness and density of the composite film significantly increase in the CNTF-10/Cu-80 system. The increase in the electromagnetic shielding effectiveness is less than the increase in the density and thickness, so the SSE_t value will decrease; thus, we selected 60 min as the best electrochemical deposition time for the subsequent research.

We further verified that the EMI efficiency of this sandwich structure is much better than that of a structure with a metal layer only on one side. Typically, the Cu NP layers will be deposited on both sides of CNTF by using our electrochemical deposition methods. Hence, we utilize an automatic vacuum ion sputtering method to deposit Cu layers on the single side and both sides of the CNTF films to explore the advantage of the sandwich structure. The images are shown in Figure S4 of the supplemental information. The sputtering time of one side of Cu layer was 20 min, and the thickness of one side of the Cu layer was 300 nm. As clearly shown in Figures 3E and 3F, the EMI efficiency of this sandwich structure is better than that of the structure only with metal layer on one side. It also should be noted that compared with a low deposition velocity of automatic vacuum ion sputtering, our facile electrochemical deposition method is much more efficient for the deposition of Cu NP layer.

Furthermore, we deposited Ni NP on the CNTF to demonstrate whether the choice of metal material has a great impact on the EMI efficiency. The absolute EMI efficiency of Cu NP/CNTF/Cu NP composite materials is 1.1 times higher than that of Ni NP/CNTF/Ni NP composite materials. Detailed data for the CNTF/Ni NP composite materials are shown in Figure S5 and Table S1 of the supplemental information. We also tested contact angle of CNTF/Cu NP and CNTF/Ni NP composite film. The more hydrophobic behavior for system with longer deposition time, the same trend on these two types of composite film, as shown in Figure S6 of the supplemental information.

Next, we further studied the influence of the densified structure of CNTF on the electromagnetic shielding efficiency (Figure 4A). We utilized electrochemical deposition method to deposit Cu NP layers (deposition time = 60 min) on the CNTF with different densified thicknesses. A more compact CNTF (upper inset images of Figure 4B) resulted, with a decrease in film thickness from 30 to 10 μm and an enhancement of SSE_t from 1.12×10^5 dB cm^2 g^{-1} to 2.17×10^5 dB cm^2 g^{-1}. This indicated a microstructural change in the CNTF; that is, the compact stacking of CNTs and improved interaction between tubes played a dominant role in determining the EMI shielding performance of the CNTF. Hence, by these comparisons, we obtained the optimal composite system (CNTF-10/Cu-60) with the highest absolute electromagnetic shielding efficiency.

We further analyzed the electromagnetic shielding performance of CNTF-10/Cu and observed a gradual increase in both SE_A and SE_T with the deposition time (Figure 3C). SE_A contributes more significantly to the overall electromagnetic shielding efficiency of the material, while SE_R remains essentially unchanged. In general, due to the occurrence of reflection losses before absorption losses, high values of SE_A primarily indicate the attenuating effect of the shielding material on incoming electromagnetic waves entering its interior. It is evident that internal absorption losses make a major contribution to the total EMI SE, mainly attributed to dielectric losses between adjacent Cu-plated CNT fibers and multiple reflections within the porous structure. The interaction between electric dipoles in the material and the electromagnetic field enhances absorption losses (as shown in Figure 4C, ② and ④). From the perspective of electromagnetic energy, to further identify the primary electromagnetic shielding mechanism in CNTF/Cu composite materials, including absorption coefficient (A), reflection coefficient (R), and transmission coefficient (T), we compared the average EMI shielding performance in the X-band for samples with different electrochemical deposition times, as shown in Figure S6. In CNTF-10/Cu composite materials, the R value is consistently greater than the A value. Experimental results indicate that reflection losses are caused by the mismatch between the inherent impedance of the deposited Cu layer and spatial impedance. This mismatch results from the interaction of charged particles (free electrons or holes) in the metal Cu layer with the electromagnetic field (as shown in Figure 4C, ① and ③), further illustrating that the electromagnetic shielding mechanism in CNTF/Cu composite materials involves primarily reflection, with absorption playing a synergistic role.

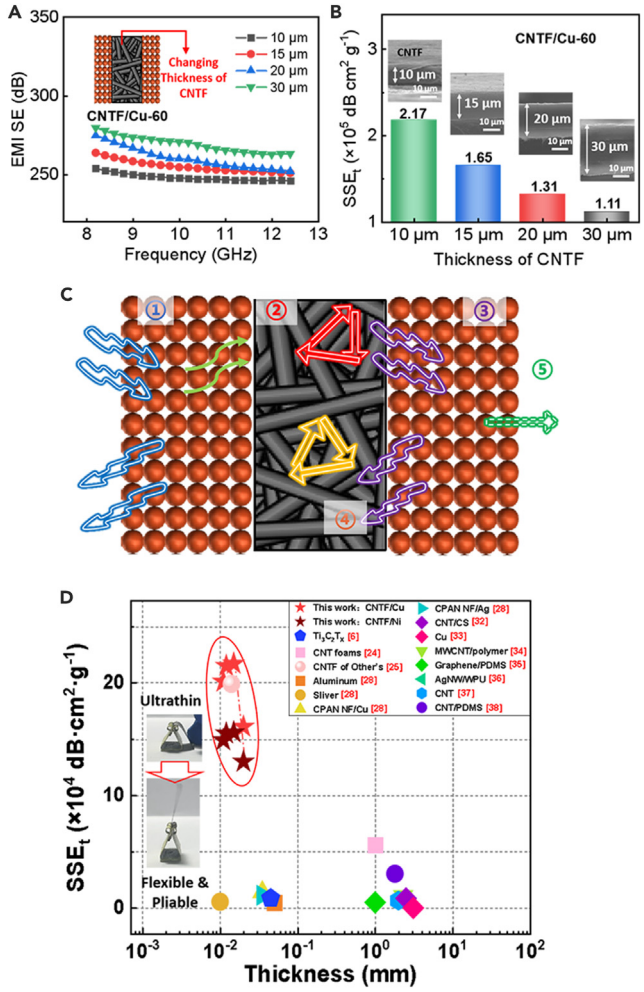

Figure 4. Electromagnetic shielding mechanism of composite thin films

(A) Electromagnetic shielding performance of CNTF with different thicknesses.

(B) Absolute electromagnetic shielding performance of CNTF with different thicknesses. The Cu NP layers all have the same thickness in these systems.

(C) Mechanism for the enhanced electromagnetic shielding efficiency of our CNTF/Cu NP composite films.

(D) Comparison of electromagnetic shielding performance with other materials and CNT films or foams of other groups, showing that our CNTF/Cu NP composite films have highest electromagnetic interference shielding effectiveness while also having the lower thicknesses.

These lightweight, ultrathin CNTF/Cu NP composite films also have excellent, flexible and pliable mechanical properties, as shown in the inset image of Figure 4D. Notably, in comparison with currently reported EMI materials,[6,9,26,27,30,34,36–40] we prepared ultrathin CNTF/Cu NP composite films exhibit an ultrahigh EMI SE of approximately 248 dB at a thickness of approximately 15 μm (the metal thickness of the two sides is ~5 μm, and the thickness of CNTF is ~10 μm). The absolute EMI shielding effectiveness, SSE_t is as high as 2.17 × 10^5 dB cm^2 g^{-1}. To the best of our knowledge, our reported absolute EMI shielding effectiveness value is the best achieved for composite EMI shielding materials with similar or greater thicknesses, and this value is also higher than the reported values of EMI SSE_t for typical pure metals.

Mechanical properties are important in the application of electromagnetic shielding materials. As our final test, we measured the mechanical properties of the composite film during bending tests. Figure 5A and Video S1 demonstrates the good mechanical flexibility of the material throughout repeated bending cycles. Figure 5B shows the stress-strain curves of CNTF and CNTF/Cu systems. It is clear to see the Cu NP layers outside benefit the mechanical property of the CNTF/Cu NP composite materials. The fracture strength of CNTF-10/Cu-20 is 19.3 MPa, with a fracture elongation of 8.03%. As the chemical deposition time extends to 80 min, the fracture strength increases to 31.7 MPa, while the fracture elongation decreases to 3.77%. The reduction in fracture elongation is minimal, and the material still maintains good mechanical properties. This is attributed to the increasing number of metal NPs on the fiber surface with the prolonged electrochemical deposition time.[41,42] The gathering of metal atoms on the CNT fiber surface enhances the sliding friction resistance between CNTs, leading to an increase in fracture strength (detailed data are in Table S2). Later, the optimal CNTF-10/Cu-60 systems were subjected to 20,000 manual

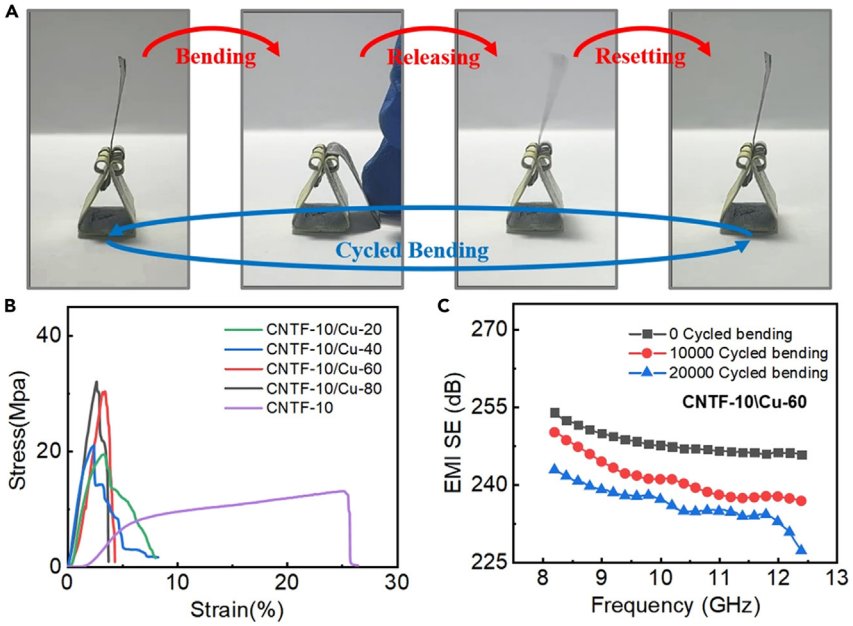

Figure 5. Mechanical properties of composite films

(A) Simplified bending experiment to show the flexible and pliable properties of CNTF/Cu NP composites.

(B) Stress-strain curves of CNTF/Cu NP composites, compared with CNTF.

(C) Electromagnetic shielding performance of CNTF/Cu NP composites after bending experiments.

operations and repeated bending to show the change in electromagnetic shielding efficiency after multiple bending cycles. After 10,000 bending cycles, the EMI SE of CNTF-10/Cu-60 decreased by 4 dB, and, as the number of bending cycles increased, the shielding efficiency gradually decreased. After 20,000 bending cycles, the EMI SE decreased by 6 dB. The results show that the film can still maintain good electromagnetic shielding performance after 20,000 times bending cycles (as shown in Figure 5C).

Conclusions

In this work, engineered sandwich-structured ultra-thin and pliable CNTF/Cu NP composite films are fabricated via a facile electrodeposition method. The excellent EMI shielding efficiency is attributed to the engineered sandwich structure of CNTF/Cu NP composite films, which have a high reflection efficiency on the outside of the Cu NP layers and the multi-reflection and adsorption efficiency from CNTF in the middle layer. Notably, the CNTF/Cu NP composite film with 15 μm thickness can achieve an excellent EMI shielding efficiency of ~248 dB and absolute EMI shielding effectiveness as high as 2.17×10^5 dB cm^2 g^{-1}, which are the best values for composite EMI shielding materials with similar or greater thicknesses. The excellent EMI shielding efficiency is attributed to the engineered sandwich structure of CNTF/Cu NP composite films, which have a high reflection efficiency on the outside Cu NP layers and the multi-reflection and adsorption efficiency of CNTF in the middle layer. Such engineered CNTF/Cu NP composite films also exhibit excellent deformation tolerance, which ensures the robust reliability of EMI shielding efficiency after a repeated bending over 20,000 cycles. Our lightweight flexible CNTF/Cu NP composite films have superior EMI shielding performance and have potential applications in aerospace, defense, and smart and wearable electronics.

STAR★METHODS

Detailed methods are provided in the online version of this paper and include the following:

- KEY RESOURCES TABLE
- RESOURCE AVAILABILITY
  - Lead contact
  - Materials availability
  - Data and code availability
- METHOD DETAILS
  - Experimental details
  - Characterization details

SUPPLEMENTAL INFORMATION

Supplemental information can be found online at https://doi.org/10.1016/j.isci.2024.109525.

ACKNOWLEDGMENTS

This work was supported by the joint SINO-GERMAN RESEARCH PROJECT (No. GZ1257), the Top-notch Academic Programs Project of Jiangsu Higher Education Institutions (TAPP), the Priority Academic Program Development of Jiangsu Higher Education Institutions (PAPD), and The National Key R&D Program of China (2022YFA1203303).

AUTHOR CONTRIBUTIONS

H. Z. and X. D. conducted the experiments. X.G. designed the experiments and wrote the paper. Z.Y. and S.R. gave suggestions and discussions.

DECLARATION OF INTERESTS

The authors declare no competing interests.

Received: November 10, 2023
Revised: January 14, 2024
Accepted: March 14, 2024
Published: April 10, 2024

REFERENCES

1. Raymond, S.K. (2002). Cellphones, radars, and health - Exposure standards for electromagnetic radiation do not adequately address current realities. IEEE Spectr *39*, 15–16.
2. Bann, R., Grosse, Y., Lauby-Secretan, B., Ghissassi, F., Bouvard, V., Benbrahim-Tallaa, L., Guha, N., Islami, F., Galichet, L., and Straif, K. (2011). Carcinogenicity of radio frequency electromagnetic fields. Lancet Oncol. *12*, 624–626.
3. Schüz, J., and Ahlbom, A. (2008). Exposure to electromagnetic fields and the risk of childhood leukaemia: a review. Radiat. Protect. Dosim. *132*, 202–211.
4. Grellier, J., Ravazzani, P., and Cardis, E. (2014). Potential health impacts of residential exposures to extremely low frequency magnetic fields in Europe. Environ. Int. *62*, 55–63.
5. Xiong, R., Hu, K., Grant, A.M., Ma, R., Xu, W., Lu, C., Zhang, X., and Tsukruk, V.V. (2016). Ultrarobust transparent cellulose nanocrystal-graphene membranes with high electrical conductivity. Adv. Mater. *28*, 1501–1509.
6. Shahzad, F., Alhabeb, M., Hatter, C.B., Anasori, B., Man Hong, S., Koo, C.M., and Gogotsi, Y. (2016). Electromagnetic interference shielding with 2D transition metal carbides (MXenes). Science *353*, 1137–1140.
7. Wang, X.X., Cao, W.Q., Cao, M.S., and Yuan, J. (2020). Assembling nano-microarchitecture for electromagnetic absorbers and smart devices. Adv. Mater. *32*, 2002112.
8. Shen, B., Li, Y., Yi, D., Zhai, W., Wei, X., and Zheng, W. (2016). Microcellular graphene foam for improved broadband electromagnetic interference shielding. Carbon *102*, 154–160.
9. Zeng, Z., Jin, H., Chen, M., Li, W., Zhou, L., Xue, X., and Zhang, Z. (2017). Microstructure design of lightweight, flexible, and high electromagnetic shielding porous multiwalled carbon nanotube/polymer composites. Small *13*, 1701388.
10. Wan, Y., Xiong, P., Liu, J., Feng, F., Xun, X., Gama, F.M., Zhang, Q., Yao, F., Yang, Z., Luo, H., and Xu, Y. (2021). Ultrathin, strong, and highly flexible $Ti_3C_2T_x$ MXene/bacterial cellulose composite films for high-performance electromagnetic interference shielding. ACS Nano *15*, 8439–8449.
11. Fu, H., Yang, Z., Zhang, Y., Zhu, M., Jia, Y., Chao, Z., Hu, D., and Li, Q. (2020). SWCNT-modulated folding-resistant sandwich-structured graphene film for high-performance electromagnetic interference shielding. Carbon *162*, 490–496.
12. Song, P., Liu, L., Fu, S., Yu, Y., Jin, C., Wu, Q., Zhang, Y., and Li, Q. (2013). Striking multiple synergies created by combining reduced graphene oxides and carbon nanotubes for polymer nanocomposites. Nanotechnology *24*, 125704.
13. Wu, Z.P., Liu, T., Chen, D.M., Wu, G., Wang, Q.H., Yin, Y.H., Li, Y.S., Xu, Q.F., and Krishamurthy, A. (2016). A facile method to improving the electromagnetic interference shielding of a free-standing and foldable carbon nanotube mat. RSC Adv. *6*, 62485–62490.
14. Ma, Y., Lv, C., Tong, Z., Zhao, C.F., Li, Y.S., Hu, Y.Y., Yin, Y.H., Liu, X.B., and Wu, Z.P. (2020). Single-layer copper particles integrated with a carbon nanotube film for flexible electromagnetic interference shielding. J. Mater. Chem. C *8*, 9945–9953.
15. Jia, H., Kong, Q.Q., Yang, X., Xie, L.J., Sun, G.H., Liang, L.L., Chen, J.P., Liu, D., Guo, Q.G., and Chen, C.M. (2021). Dual-functional graphene/carbon nanotubes thick film: Bidirectional thermal dissipation and electromagnetic shielding. Carbon *171*, 329–340.
16. Xi, J., Li, Y., Zhou, E., Liu, Y., Gao, W., Guo, Y., Ying, J., Chen, Z., Chen, G., and Gao, C. (2018). Graphene aerogel films with expansion enhancement effect of high-performance electromagnetic interference shielding. Carbon *135*, 44–51.
17. Xu, J., Li, R., Ji, S., Zhao, B., Cui, T., Tan, X., Gou, G., Jian, J., Xu, H., Qiao, Y., et al. (2021). Multifunctional graphene microstructures inspired by honeycomb for ultrahigh performance electromagnetic interference shielding and wearable applications. ACS Nano *15*, 8907–8918.
18. Lee, J.S., Kim, J.W., Lee, J.H., Son, Y.K., Kim, Y.B., Woo, K., Lee, C., Kim, I.D., Seok, J.Y., Yu, J.W., et al. (2023). Flash-Induced High-Throughput Porous Graphene via Synergistic Photo-Efects for Electromagnetic Interference Shielding. Nano-Micro Lett. *15*, 191.
19. Nan, Z., Wei, W., Lin, Z., Chang, J., and Hao, Y. (2023). Flexible Nanocomposite Conductors for Electromagnetic Interference Shielding. Nano-Micro Lett. *15*, 172.
20. Kim, H.R., Fujimori, K., Kim, B.S., and Kim, I.S. (2012). Lightweight nano fibrous EMI shielding nanowebs prepared by electro spinning and metallization. Compos. Sci. Technol. *72*, 1233–1239.
21. Geetha, S., Satheesh Kumar, K.K., Rao, C.R.K., Vijayan, M., and Trivedi, D.C. (2009). EMI shielding: methods and materials-A review. J. Appl. Polym. Sci. *112*, 2073–2086.
22. Jiang, D., Murugadoss, V., Wang, Y., Lin, J., Ding, T., Wang, Z., Shao, Q., Wang, C., Liu, H., Lu, N., et al. (2019). Electromagnetic interference shielding polymers and nanocomposites - A review. Polym. Rev. *59*, 280–337.
23. Gupta, S., and Tai, N.H. (2019). Carbon materials and their composites for electromagnetic interference shielding effectiveness in X-band. Carbon *152*, 159–187.
24. Li, Z.W., Fang, J.W., Mi, Y.Q., Liu, T., Yao, D.K., Zheng, Y.P., Fang, J.Y., Yin, Y.H., Liu, X.B., Li, Y.S., and Wu, Z.P. (2022). Carbon Nanotube-Fastened Graphene Composites with Bubble-Induced Multi reflections for Electromagnetic Interference Shielding with Water Repellence. ACS Appl. Nano Mater. *5*, 12926–12934.
25. Micheli, D., Apollo, C., Pastore, R., and Marchetti, M. (2010). X-Band microwave characterization of carbon-based

nanocomposite material, absorption capability comparison and RAS design simulation. Compos. Sci. Technol. *70*, 400–409.

26. Yu, Y., Chao, Z., Gong, Q., Li, C., Fu, H., Lei, F., Hu, D., and Zheng, L. (2021). Tailoring hierarchical carbon nanotube cellular structure for electromagnetic interference shielding in extreme conditions. Mater. Des. *206*, 109783.
27. Wan, Y.J., Wang, X.Y., Li, X.M., Liao, S.Y., Lin, Z.Q., Hu, Y.G., Zhao, T., Zeng, X.L., Li, C.H., Yu, S.H., et al. (2020). Ultrathin densified carbon nanotube film with "Metal-like" conductivity, superior mechanical strength, and ultrahigh electromagnetic interference shielding effectiveness. ACS Nano *14*, 14134–14145.
28. Ji, K., Zhao, H., Zhang, J., Chen, J., and Dai, Z. (2014). Fabrication and electromagnetic interference shielding performance of open-cell foam of a Cu–Ni alloy integrated with CNTs. Appl. Surf. Sci. *311*, 351–356.
29. Pande, A., Gairola, P., Sambyal, P., Gairola, S.P., Kumar, V., Singh, K., and Dhawan, S.K. (2017). Electromagnetic shielding behaviour of polyaniline using Red Mud (Industrial Waste) as filler in the X - band (8.2-12.4 GHz) frequency range. Metal. Chem. Phys. *189*, 22–27.
30. Ji, H., Zhao, R., Zhang, N., Jin, C., Lu, X., and Wang, C. (2018). Lightweight and flexible electrospun polymer nanofiber/metal nanoparticles hybrid membrane for high-performance electromagnetic interference shielding. NPG Asia Mater. *10*, 749–760.
31. Zhang, Y., Pan, T., and Yang, Z. (2020). Flexible polyethylene terephthalate/polyaniline composite paper with bending durability and effective electromagnetic shielding performance. Chem. Eng. J. *389*, 124433.
32. Wei, Q., Pei, S., Qian, X., Liu, H., Liu, Z., Zhang, W., Zhou, T., Zhang, Z., Zhang, X., Cheng, H.M., and Ren, W. (2020). Superhigh electromagnetic interference shielding of ultrathin aligned pristine graphene nanosheets film. Adv. Mater. *32*, 1907411.
33. Shen, B., Li, Y., Zhai, W., and Zheng, W. (2016). Compressible graphene-coated polymer foams with ultralow density for adjustable electromagnetic interference (EMI) shielding. ACS Appl. Mater. Interfaces *8*, 8050–8057.
34. Li, M.Z., Jia, L.C., Zhang, X.P., Yan, D.X., Zhang, Q.C., and Li, Z.M. (2018). Robust carbon nanotube foam for efficient electromagnetic interference shielding and microwave absorption. J. Colloid Interface Sci. *530*, 113–119.
35. Wang, W., Zhang, L., Tong, S., Li, X., and Song, W. (2009). Three-dimensional network films of electrospun copper oxide nanofibers for glucose determination. Biosens. Bioelectron. *25*, 708–714.
36. Shui, X., and Chung, D.D.L. (1997). Nickel filament polymer-matrix composites with low surface impedance and high electromagnetic interference shielding effectiveness. J. Electron. Mater. *26*, 928–934.
37. Chen, Z., Xu, C., Ma, C., Ren, W., and Cheng, H.M. (2013). Lightweight and flexible Graphene foam composites for high-performance electromagnetic interference shielding. Adv. Mater. *25*, 1296–1300.
38. Zeng, Z., Chen, M., Pei, Y., Seyed Shahabadi, S.I., Che, B., Wang, P., and Lu, X. (2017). Ultralight and flexible polyurethane/silver nanowire nanocomposites with unidirectional pores for highly effective electromagnetic shielding. ACS Appl. Mater. Interfaces *9*, 32211–32219.
39. Hong, X., and Chung, D.D.L. (2017). Carbon nanofiber mats for electromagnetic interference shielding. Carbon *111*, 529–537.
40. Lu, D., Mo, Z., Liang, B., Yang, L., He, Z., Zhu, H., Tang, Z., and Gui, X. (2018). Flexible, lightweight carbon nanotube sponges and composites for high-performance electromagnetic interference shielding. Carbon *133*, 457–463.
41. Li, Y.L., Kinloch, I.A., and Windle, A.H. (2004). Direct spinning of carbon nanotube fibers from chemical vapor deposition synthesis. Science *304*, 276–278.
42. Xu, J., Gong, X., Yong, Z., and Ramakrishna, S. (2020). Construction of various nanostructures on carbon nanotube films. Mater. Today Chem. *16*, 100253.

STAR★METHODS

KEY RESOURCES TABLE

REAGENT or RESOURCE	SOURCE	IDENTIFIER
Chemicals, peptides, and recombinant proteins		
Copper sulfate pentahydrate	Aladdin	CAS:7758-99-8
Sodium citrate dihydrate	Aladdin	CAS:6132-04-3
Polyethylene glycol	Aladdin	CAS:25322-68-3
Nickel sulfate hexahydrate	Aladdin	CAS:10101-97-0
Boric acid	Aladdin	CAS:10043-35-3
Other		
X-ray Diffractometer (XRD)	Rigaku D	
Scanning Electron Microscope (SEM)	Phenom ProX	
Vector Network Analyzer (EMI SE)	ZNB20	
Single-Fiber Tensile Testing Machine	XS (08) XG-50	
Direct Current Resistance Tester	XS (20A)	
Linear Motor	E1100 - CO - XC	

RESOURCE AVAILABILITY

Lead contact

Further information for resources and regents could be directed to and will be fulfilled by the lead contact, Xiaojing Gong (gongxiaojing2018@cczu.edu.cn).

Materials availability

This study does not generate new unique reagents.

Data and code availability

- All requested data is available in this paper will be shared by the lead contact upon request.
- This paper does not report original code.
- Any additional information required to reanalyze the data reported in this paper is available from the lead contact upon request.

METHOD DETAILS

Experimental details

Preparations of the CNTF

Carbon nanotube films are commonly prepared by float catalyst chemical vapor deposition. An ethanol solution containing 2% ferrocene and 1% thiophene was injected by a programmable syringe into a tubular reactor as a carbon source and catalyst for the growth of carbon nanotubes. Hydrogen gas (2000 sccm) was injected as a carrier gas. The growth of the carbon nanotubes occurred at a temperature around 800°C. Ethanol, thiophene, and ferrocene were used as raw materials. The carbon nanotubes were organized into a thin aerogel hollow tube, blown out of the reactor tube with the help of flowing gas, and then continuously collected on a roller.

Preparations of the densified CNTF

To create a series of CNTFs with different thickness, we compressed the carbon nanotube aerogel to obtain the CNTFs and sprayed alcohol on the surface to compact them. We then placed them in a FW-4/4A press machine for further densification processing by applying different pressures, resulting in densified carbon nanotube films with thicknesses of 10 μm, 15 μm, 20 μm, and 30 μm. To clarify the discussion in Section 3, we denoted these samples with different densified thicknesses as *CNTF-10*, *CNTF-15*, *CNTF-20*, and *CNTF-30*, respectively.

Preparations of the CNTF/Cu NP composite films using electrochemical deposition of copper nanoparticle layers on CNTFs

The roll of CNTF with densified thickness was first placed in a plasma cleaner at a power of 70 W for 120 s after pretreatment to avoid the dispersion or corrosion of carbon nanotubes during electrolysis. Copper nanoparticle layers were grown on the surface of the pretreated

carbon nanotube film. The electrolyte was an aqueous solution of copper sulfate $CuSO_4$ (0.03 M), sodium citrate $Na_3C_6H_5O_7$ (0.05 M), boric acid H_3BO_3 (0.5 M), and polyethylene glycol (6 g/L). The electrochemical deposition temperature was 75°C, the constant potential was -0.92 V, and the pH was adjusted to 8 with NaOH. The electrochemical deposition lasted for 20, 40, 60 or 80 min. To clarify the discussion in Section 3, we denoted these samples with different decomposition times as *CNTF/Cu-20*, *CNTF/Cu-40*, *CNTF/Cu-60*, and *CNTF/Cu-80*, respectively (with the same thickness of CNTF). The electrolyte was continuously stirred at a speed of 200 rpm throughout the reaction. The electrochemical deposition potential could be adjusted by an electrochemical workstation (CHI 660E, Chenhua, China). A three-electrode system was used, with the carbon nanotube film as the working electrode, a platinum plate as the counter electrode, and Ag/AgCl as the reference electrode. After the reaction, the sample surface was rinsed with deionized water to remove any possible solvent residues, and then dried with argon gas and placed in an oven at 60°C for 30 min to remove the residual moisture in the gap of the sample.

Preparations of the CNTF/Ni NP composite films using electrochemical deposition of nickel nanoparticle layers on CNTFs

To exploit the influence of metal materials on EMI shielding efficiency. we also prepared Ni nanoparticle layers on CNTF for comparison with copper nanoparticle layers. The roll of CNTF was first placed in a plasma cleaner at a power of 70 W for 120 s after pretreatment to avoid the dispersion or corrosion of carbon nanotubes during electrolysis. Nickel nanoparticle layers were grown on the surface of the pretreated carbon nanotube film. The electrolyte was an aqueous solution of nickel sulfate NiSO4 (0.05 M) and boric acid H3BO3 (0.2 M). The electrochemical deposition temperature was 60°C, the constant potential was -1.7 V, and the electrochemical deposition lasted for 20, 40, 60 or 80 min. The electrolyte was continuously stirred at a speed of 200 rpm throughout the reaction. The electrochemical deposition potential could be adjusted by an electrochemical workstation (CHI 660E, Chenhua, China). A three-electrode system was used, with the carbon nanotube film as the working electrode, a platinum plate as the counter electrode, and Ag/AgCl as the reference electrode. After the reaction, the sample surface was rinsed with deionized water to remove any possible solvent residues, and then dried with argon gas and placed in an oven at 60°C for 30 min to remove the residual moisture in the gap of the sample. For clear discussions, we have denoted these samples with different decomposition time as *CNTF/Ni-20*, *CNTF/Ni-40*, *CNTF/Ni-60*, *CNTF/Ni-80*, respectively.

Characterization details

The microstructure and structure of the prepared CNTF/Cu NP composite films were investigated via scanning electron microscopy (SEM, Phenom ProX, Holland) at an accelerating voltage of 15.0 kV. The phase and crystalline structure of the composite films were determined by X-ray diffraction (Rigaku, Japan) with Cu Kα radiation, λ = 1.54 Å. The EMI shielding effeciency were tested by a vector network analyzer (Rohde & Schwarz Co., Ltd. ZNB20) via waveguide method, frequency range: 8.2-12.4GHz. The mechanical properties of the composite films (width = 10 mm) were evaluated by using a single-fiber tensile testing machine (XS (08) XG-50, Shanghai XuSai Technology Co., Ltd.) at a grip separation rate of 5 mm·min^{-1} and a gauge length of 15 mm. The tensile strength and fracture elongation were evaluated using stress-strain curves. The conductivity (σ) of all the composite films was measured using a direct current resistance tester (XS (20A), Shanghai XuSai Technology Co., Ltd.). The results were averaged over at least five different regions of the sample to ensure the accuracy of the conductivity measurement. A linear motor (E1100 - CO - XC, Suzhou Kereli Motor Co., Ltd.) was used for bending experiments on the composite film. The composite film was fixed on the bending device and subjected to reciprocating bending tests with a bending angle of 90°. Bending cycles of 10,000 and 20,000 were performed. We utilize an automatic vacuum ion sputtering instrument (CIS-400-Shanghai Zhongbin) to deposit copper layer on the single side and both sides of the CNTF films to explore the advantage of sandwich structure. The sputtering time of one side of copper layer was 20 minutes, and the thickness of one side of the copper layer was 300 nm.